Evaluation on thermodynamic compatibility between high density ceramic nuclear reactor fuels UX(X=C,N) and light-water reactor cladding materials (Zr and SiC)*

Ying Yang[1,†] and Andrew Nelson[2]

[1]*Material Science and Technology Division, Oak Ridge National Laboratory, Oak Ridge, TN 37831, USA*
[2]*Nuclear Energy and Fuel Cycle Division, Oak Ridge National Laboratory, Oak Ridge, TN 37831, USA*

High-density fuels, including uranium monocarbide (UC), uranium mononitride (UN), and uranium carbonitride (UCN) formed from carbon impurities during UN fabrication, have recently attracted attention for light-water reactor (LWR) applications due to their potential for increased ^{235}U loading at a fixed enrichment, high thermal conductivity, and elevated melting temperatures. Despite these favorable properties, several performance aspects must be evaluated before these lesser-studied uranium compounds can become viable LWR fuel forms. This study is the first to perform thermodynamic calculations evaluating the thermal stability of pure UC and UN in a closed system representative of pressurized water reactor coolant. The results indicate that neither UN nor UC is thermodynamically stable in aqueous electrochemical environments during a cladding breach. Subsequently, the potential interactions between UN and UCN with Zr or SiC claddings were systematically evaluated using a newly developed U–Zr–Si–C–N thermodynamic database constructed through the CALPHAD approach and validated with literature data. Interfacial stability for UN/Zr, UC/Zr, UN/SiC, and UC/SiC couples was assessed by calculating isothermal sections of U–Zr–N, U–Zr–C, U–Si–C, and U–Si–C–N systems at 1500, 1000, and 500 °C, as well as isopleth sections of U($C_{0.3}N_{0.7}$)–Zr. The results predict that the UN–Zr interface produces multiple reaction layers including bcc(U,Zr), UZr_2, hcp(Zr,N), and fcc(U,Zr)N phases, whereas the UC–Zr system forms a single ZrC layer. Improved thermodynamic stability is predicted for both UC and UN when in contact with SiC cladding, as both remain in equilibrium at all evaluated temperatures. Carbon impurities within UN are not expected to detrimentally affect fuel–cladding interactions for either Zr or SiC under the studied conditions.

Keywords: Nuclear fuel, Thermodynamics, Phase diagrams

I. INTRODUCTION

High-density nuclear fuels, defined as compounds or fuel architectures possessing greater uranium density than uranium dioxide (UO_2), have recently attracted attention for light-water reactor (LWR) applications [1]. Replacing UO_2 with a higher-density fuel enables increased ^{235}U loading at a fixed enrichment, allowing extended cycle length, higher reactor power, or compensation for potential neutronic penalties associated with alternative cladding materials [2]. These advantages translate to economic and operational improvements, particularly when combined with higher enrichment fuels [3, 4].

Numerous uranium compounds offering higher uranium density than UO_2 have been proposed. Metallic (e.g., U–Zr and U–Mo) and intermetallic (e.g., U–Si and U–B) systems have been investigated [5–7], but recent research has focused on uranium mononitride (UN) as the most promising high-density fuel form [8]. Uranium mononitride belongs to the broader "MX" family of fuel systems, where M is typically uranium, and X is carbon, nitrogen, or their mixtures. Because plutonium is not currently prioritized for commercial LWR use in the United States, the relevant subset includes uranium monocarbide (UC), uranium mononitride (UN), and uranium carbonitride (UCN), the latter forming from carbon impurities during UN fabrication [6, 7]. In addition to providing a higher uranium density, these fuels also offer higher thermal conductivities and maintain solid-state stability to high temperatures [9, 10].

Despite these favorable properties, numerous performance aspects must be evaluated before these lesser-studied uranium compounds can be considered viable for LWR deployment. Irradiation testing is essential to assess swelling, fission gas release, fission product behavior, and microstructural evolution of UN under reactor conditions. However, integral irradiation experiments are costly and time-consuming. To accelerate development, programs increasingly employ "accelerated fuel qualification," emphasizing computational screening to eliminate unsuitable candidates and guide experimental testing [11].

Thermodynamic compatibility of non-oxide fuels has already been demonstrated to be concept-limiting. Interest in U_3Si_2 fuels for LWRs was motivated for similar reasons as UC and UN: superior uranium density and high thermal conductivity. However, significant investment occurred before experimental results demonstrated poor compatibility with water coolants [12]. This response poses a significant concern to reactor operation in the event of a cladding breach experienced under even normal operating conditions [2]. Thermodynamic screening of proposed fuel forms with water coolants as used by pressurized water reactors (PWRs)

† Corresponding author, Ying Yang, P.O. Box 2008, MS-6115, Oak Ridge, TN 37831-6115, 865-576-4427, yangying@ornl.gov

is therefore a basic step to screen for performance issues.

Fuel–cladding thermochemical compatibility is another important aspect of nuclear fuel design. In most reactor designs incorporating monolithic fuels, fuel swelling or relocation of the fuel will couple with inward creep of the cladding driven by coolant pressure to place the fuel and cladding in close contact at some point in the designed service life of the fuel. Deleterious reactions between elemental constituents of the fuel and cladding have the potential to degrade the mechanical strength of the cladding or induce other concerns. This has long been appreciated as an issue for fast reactor fuels [13, 14]. Conversely, the chemical interaction layer that forms when UO_2 comes into contact with Zr cladding are generally not viewed as significant to commercial LWR reactor operation [15, 16]. The extent and significance of possible interfacial reactions for new fuel or cladding materials is presently acknowledged as an unknown for advanced LWR fuels [17] and will determine the success of fuel systems to support new reactor designs [18].

Evaluation of the extent of concern posed by fuel–cladding interaction is usually limited to experimental study of unirradiated diffusion couples [19, 20] and examination of fuel–cladding contact regions following integral irradiation testing [21]. Experimental observations are ultimately necessary, as interdiffusion kinetics, radiation-enhanced diffusion, and the complicating role of fission product effects are challenging to predict. However, evaluation of experimental outcomes are informative only regarding the specific test conditions.

The present work was conceived to provide a screening study of the predicted thermodynamic behavior of systems that will govern the performance of UN when used as an LWR fuel. Uranium mononitride is the specific fuel form of focus, but UC is included to serve as an endpoint for potential carbon contamination resulting in fabrication of UCN fuels. Zirconium is chosen for the reference cladding constituent. Silicon carbide (SiC) was also chosen as a candidate cladding system, as it has been proposed for pairing with UN to yield a high performance LWR fuel [22, 23]. The CALPHAD (CALculation of Phase Diagram) approach is used to assess thermodynamic behavior [24]. The resulting phase equilibria can then be used to discuss the probable outcomes of interaction of UCN with coolant during normal operation, potential phase formation following fuel–cladding contact during normal service, and conditions at elevated temperatures where deleterious interactions may become a concern. Finally, these phase diagrams may provide insight into means of mitigating any potential concerns.

II. METHOD

The CALPHAD approach [24] was used to model the Gibbs energies for phases in the U–(C,N)–(Zr,SiC) multicomponent system. The phases included in the system are listed in Table 1.

Thermodynamic models for different phases have been discussed in detail in literature [24]. Here, those models relevant to the phases present in the current system are briefly described here. Detailed formula on Gibbs energy of phases are provided in the supplementary file. The gas phase was modeled as an ideal mixture of different molecules. The liquid phase was modeled as a substitutional solution (SS) model. The Gibbs energy of a liquid phase is described as the sum of the Gibbs energy of each molecule $\left(G_i^0(T)\right)$, weighted by the mole fraction of each molecule (x_i), the ideal configuration entropy of mixing and the excess Gibbs energy $\left(G^{EX}\right)$:

$$G_m = \sum_i \left(x_i G_i^0(T) + RTx_i \ln x_i\right) + G^E X \qquad (1)$$

The excess energy is described as

$$G^E X = \sum_i x_i \sum_j \left[L_{ij} + \sum_k x_k L_{ijk}\right] \qquad (2)$$

where L_{ij} and L_{ijk} are, respectively, binary and ternary interaction parameters. These parameters often depend linearly on temperature. In many cases, they may also depend on compositions following Redlich–Kister polynomial [25]. Equation (2) was developed by Muggianu et al. [26] and is an important extrapolation method that derives the thermodynamic properties of multicomponent alloys from the constituent binary and ternary systems.

The modeling of crystalline phases depends on the crystal structures of phases. For phases with a single set of lattice site, the Gibbs energy is described as the same way as substitutional solution model as shown in Eqs. (1) and (2). For phases with more than one sublattice, the Gibbs energy was modeled by compound energy formalism. Due to the model complexity, the mathematic equation will be described using the (U,Zr)1(C,N)1 sublattice model as an example. The (U,Zr)1(C,N)1 sublattice model is used to describe the UC, UN, ZrC and ZrN phases because these phases have the same crystal structure. The first sublattice denotes the lattice sites for metal atoms (U and Zr), and the second sublattice denotes the interstitial sites for interstitial atoms (C and N). The interstitial sites can also have other species, such as C_2, and vacancy, as shown in Table 1. Here, for the ease of model description, only C and N are included. The stochiometric coefficients of two sublattices are 1 and so the model can be simplified as (U,Zr)(C,N). The Gibbs energy is described as

$$\begin{aligned} G_m^{\varphi} = {} & y_U^I y_C^{II} G_{U:C}^{\varphi} + y_U^I y_N^{II} G_{U:N}^{\varphi} + y_{Zr}^I y_C^{II} G_{Zr:C}^{\varphi} \\ & + y_{Zr}^I y_N^{II} G_{Zr:N}^{\varphi} + RT\left(y_U^I \ln y_U^I + y_{Zr}^I \ln y_{Zr}^I\right) \\ & + RT\left(y_C^{II} \ln y_C^{II} + y_N^{II} \ln y_N^{II}\right) + G^{EX} \end{aligned} \qquad (3)$$

where y_i^n denotes the site fraction of element i in the nth sublattice, $G_{i:j}^{\varphi}$ is the Gibbs energy of the compound with a φ structure in which the first sublattice is fully occupied by element i and the second sublattice by element j. The configurational entropy is described in terms of site fractions:

$$\begin{aligned} G^{EX} = {} & y_U^I y_C^{II} y_N^{II} L_{U:C,N} + y_{Zr}^I y_C^{II} y_N^{II} L_{Zr:C,N} \\ & + y_U^I y_{Zr}^I y_C^{II} L_{U,Zr:C} + y_U^I y_{Zr}^I y_N^{II} L_{U,Zr:N} \end{aligned} \qquad (4)$$

where $L_{i:j,k}$ means the interaction parameter between elements j and k in the second sublattice when the first sublattice is fully occupied by element i. The remaining three

Table 1. Phases modeled in the current study together with their models, constituents and crystal structures

Phase	Model	Constituents	Crystal structure
Gas	SS	C, C_2, C_3, C_4, N, N_1Si_1, N_1Si_2, N_1Zr_1, N_2, N_3, Si, Si_2, Si_3, U, Zr, Zr_2	—
Liquid	SS	C, N, Si, U, Zr	—
bcc(C,N,U,Si,Zr)	CEF	(Si,U,Zr)(C,N,VA)	cI2, $Im\bar{3}m$
hcp(C,N,Si,U,Zr)	CEF	(Si,U,Zr)(C,N,VA)	hP2, $P6_3/mmc$
ORTHORHOMBIC_A20(O(U))	SS	(U,Zr)	oC4, $Cmcm$
TETRAGONAL_U (T(U))	SS	(U,Zr)	tP30, $P4_2/mnm$
GRAPHITE_A9 (Gra)	LC	C	hP4, $P6_3/mcm$
DIAMOND_A4 (Dia)	SS	(C,Si)	cF8, $Fd\bar{3}m$
UC, UN, ZrC, βUC_2	CEF	(U,Zr)(C,C_2,N,Va)	$Fm\bar{3}m$
U_2C_3	LC	(U)2(C)3	$I\bar{4}3d$
UC_2	CEF	(U)(C,Va)	$I4/mmm$
U_2N_3	LC	(U)2N(3)	$P\bar{3}m1$
U_3Si	LC	(U)3(Si)	cP4, $Pm\bar{3}m$
USi	LC	(U)(Si)	oP8, $Pnma$
U_3Si_5	LC	(U)3(Si)5	hP3, $P6/mmm$
$USi_1.88$	LC	(U)(Si)1.88	tI12, $I4_1/amd$
USi_3	LC	(U)(Si)3	cP4, $Pm\bar{3}m$
UZr	CEF	(U,Zr)(U,Zr)	hP3, $P6/mmm$
U_3Si_2	CEF	(U,Zr)3(Si)2	tP10, $P4/mbm$
CSi	LC	(C)(Si)	cP8, $F\bar{4}3m$
N_4Si_3	LC	(N)4(Si)3	hP28, $P31c$
T1: $U_3Si_2C_2$	LC	(U)3(Si)2(C)2	tI14, $I4/mmm$
T2: $U_{20}Si_{16}C_3$	LC	(U)20(Si)16(C)3	hP39, $P6/mmm$

SS: substitutional solution, CEF: compound energy formalism, LC: line compound.

interaction parameters in Eq. (4) have the similar meaning. Like those parameters in Eq. (2), these parameters are also dependent on temperature and composition.

The compound energy formalism is mainly used to describe a crystalline phase with a range of homogeneity; in other words, a phase that is not strictly ordered. For crystalline phases whose composition is strictly at stoichiometric coefficient (e.g., A_mB_n), the Gibbs energy is described by line compound model:

$$G_{A_mB_n} = mG^0_A + nG^0_B + \Delta G_f \quad (5)$$

where ΔG_f is the formation energy of the compound and can vary as a function of temperature.

The models used for each phase in this work are listed in Table 1. The model parameters were obtained by simultaneously evaluating all available thermochemical and constitutional data for the system until these data can be reproduced from model-calculated results. The Gibbs energy function for a phase in a multicomponent system is built upon the constituent binary and ternary phases. The Gibbs energies of phases for pure elements and molecules in the gas phase were taken for SGTE pure element and SSUB3 thermodynamic database. For the UC/Zr, UN/Zr, UC/SiC and UN/SiC couples to be evaluated, thermodynamic models for phases in the following eight binaries were required: U–C, U–N, U–Si, U–Zr, Zr–C, Zr–N, Si–C, and Si–N. These binary systems have been thermodynamically modeled in literature [27–34]. These published model parameters were evaluated and compiled into the current self-consistent thermodynamic database. Phase diagrams for these binary systems were calculated from the database and shown in Fig. 1, consistent with those published in literature [27–34].

To evaluate thermodynamic compatibility of UC/Zr, UN/Zr, UC/SiC and UN/SiC, thermodynamic models on the Gibbs energies of phases in the U–C–Zr, U–N–Zr, U–C–Si and U–N–Si–C ternary and quaternary systems were needed. The thermodynamic models of ternary phases were first derived through extrapolation from those phases in constituent binary systems, and then the derived models were used to calculate phase diagrams. If the calculated phase diagrams agree satisfactorily with available experimental data, we will use the derived models to predict phase equilibria in the uninvestigated composition and temperature region. If not, we will optimize ternary interaction parameters until satisfactory agreement with experimental data is reached. And then, the optimized model parameters will be used to predict phase equilibria in the uninvestigated composition and temperature region. There is no ternary experimental data for U–N–Zr and U–N–Si–C systems; therefore, for these two systems, only predicted phase diagrams will be presented. For U–C–Zr and U–C–Si, there were limited experimental phase equilibrium data available for comparison. Thermodynamic description of the U–C–N system was derived from extrapolation of binary systems, and the results are consistent with literature data [35].

In the absence of direct experimental validation for the U–N–Zr and U–N–Si–C systems, an indirect validation strategy was employed. The thermodynamic models for these higher-order systems are extrapolated from experimentally validated constituent binary and ternary systems, ensuring that their phase equilibria are physically constrained by experimentally verified phase boundaries. This hierarchical approach to CALPHAD database development—anchoring higher-order system predictions in validated lower-order descriptions—is

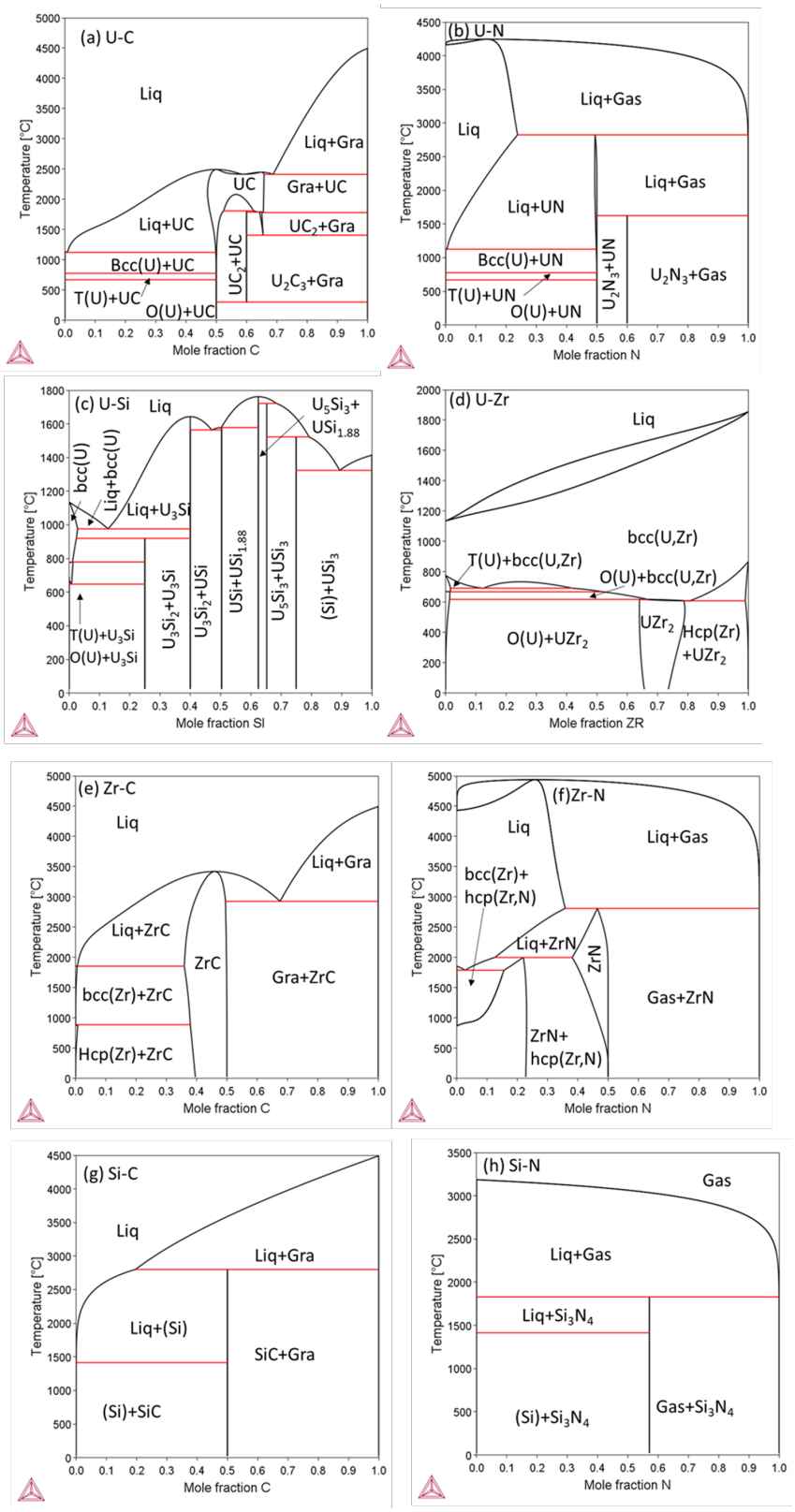

Fig. 1. Calculated binary phase diagrams from the currently developed database that compiles thermodynamics models for constitutent binaries (a) U–C [29], (b) U–N [34], (c) U–Si [27], (d) U–Zr [31], (e) Zr–C [30], (f) Zr–N [32], (g) Si–C [28], and (h) Si–N [33].

well-established in the thermodynamic modeling community [36].

In addition to evaluation on the compatibility between fuel and cladding materials, screening on thermodynamic reactions between UCN and water coolants under PWR conditions was also performed in this work. The Pourbaix diagrams of pure UC and UN in high-temperature, high-pressure water in a closed system were calculated to identify the resulting products at equilibrium. Specifically, the thermocalc software package with the Aqueous Solution database (AQS2) and pure substance database (SSUB3) were used for extracting thermodynamic quantities and performing equilibrium calculations [37]. The database was developed for calculations of thermodynamic properties of complex aqueous solutions described by the Helgeson–Kirkham–Flowers (HKF) model [38] at temperatures up to 1000 °C, pressures up to 5 kbar, and aqueous concentrations up to 6 molality.

In the sections below, we first present the calculated Pourbaix diagram of UN and UC in PWR-relevant conditions, followed by the comparison between the calculated phase diagrams and available experimental data for U–C–Zr and U–C–Si systems for validation of the developed model parameters, and then the predicted isothermal sections at 1500, 1000, and 500 °C for the U–C–Zr, U–N–Zr, U–C–Si and U–N–Si–C system using the developed and optimized model parameters. The isothermal sections at these three temperatures were chosen to be representative of three basic LWR operating conditions. 500 °C was chosen to represent the temperature of the fuel–cladding interface during normal operation. 1000 °C was chosen to represent a possible time-at-temperature off-normal scenario when UN is explored for service in a reference PWR design [39]. Finally, 1500 °C was selected as the maximum temperature that an LWR fuel would be expected to experience for a time period on the scale of hours. A loss-of-coolant accident (LOCA) or reactivity-initiated accident (RIA) subjecting the core to temperatures at or above 1500 °C would result in significant core melting and restructuring, limiting the value of thermochemical modeling performed at higher temperatures.

III. RESULTS

A. Stability of UN and UC under conditions relevant to cladding breach during normal operation

The Pourbaix calculations presented in this section were performed under several simplifying thermodynamic assumptions intended to provide a bounding equilibrium assessment of fuel stability following a cladding breach. The system was modeled as a closed thermodynamic system, meaning no mass exchange with the external environment was permitted once water ingress occurred. A fixed fuel-to-coolant molar ratio of approximately 0.005 was used to represent a localized interaction between a limited quantity of exposed fuel and a significantly larger coolant volume. The calculations were conducted assuming thermodynamic equilibrium, such that the predicted phase assemblages represent the minimum Gibbs free energy configuration without consideration of kinetic limitations. No fission products or irradiation-induced species were included in the aqueous chemistry, and the coolant was represented as pure water without corrosion products. A constant total pressure of 15 MPa, representative of PWR operating conditions, was imposed. These assumptions provide a thermodynamic bounding case relevant to extended fuel–coolant interaction under steady-state conditions, while transient accident scenarios (e.g., LOCA or RIA) and kinetic effects fall outside the scope of the present equilibrium-based analysis.

Figure 2 presents the calculated Pourbaix diagrams for (a) UN and (b) UC at 330 °C exposed to 15 MPa total pressure (a condition representative of PWR coolant). The ratio of the fuel amount to the coolant amount is 0.005. Based on the calculation results, no EH/PH combinations exist where UN or UC is stable compared to other uranium oxides or uranic acid (H_2UO_4).

B. Comparison between experimental and calculated phase diagrams

Experimental data on phase diagrams of U–C–Zr and U–C–Si were available from literature; therefore, they were used to optimize the model parameters in respective ternaries, and their comparison with the calculated results is described in detail in Sections III B 1 and III B 2. The optimized parameters were then used to predict the isothermal sections at 1500, 1000, and 500 °C, respectively. There was no well-defined experimental data for the phase diagram of U–N–Zr and U–N–SiC systems; therefore, the extrapolated thermodynamic models were used for predicting isothermal sections in Section III C.

1. The U–C–Zr ternary

Butt and Wallace reviewed the experimental data available for the U–Zr–C system [40]. They found poor agreement between the various studies. The general lack of agreement and inconsistencies between laboratories were attributed to the deficiencies in materials characterization and the difficulties associated with measurement at high temperatures. They assessed the various experimental data and postulated pseudo binary UC–$ZrC_{0.81}$ and isopleth βUC_2–ZrC. In a recent review [41], in addition to these two diagrams, isothermal section at 1700 °C was proposed based on some original experimental work [42–44]. Therefore, these diagrams were used to develop the models of the U–Zr–C ternary.

First, we calculated phase diagrams directly from extrapolated thermodynamic functions, and found disagreement with proposed experimental ones. Specifically, the extrapolated phase diagram cannot correctly reproduce the content of ZrC in the (U,Zr)C solid solution that is in equilibrium with graphite (Gra) and βUC_2. Therefore, ternary parameters were required to describe the interaction between U and Zr in the lattice sites with the interstitial sites occupied by

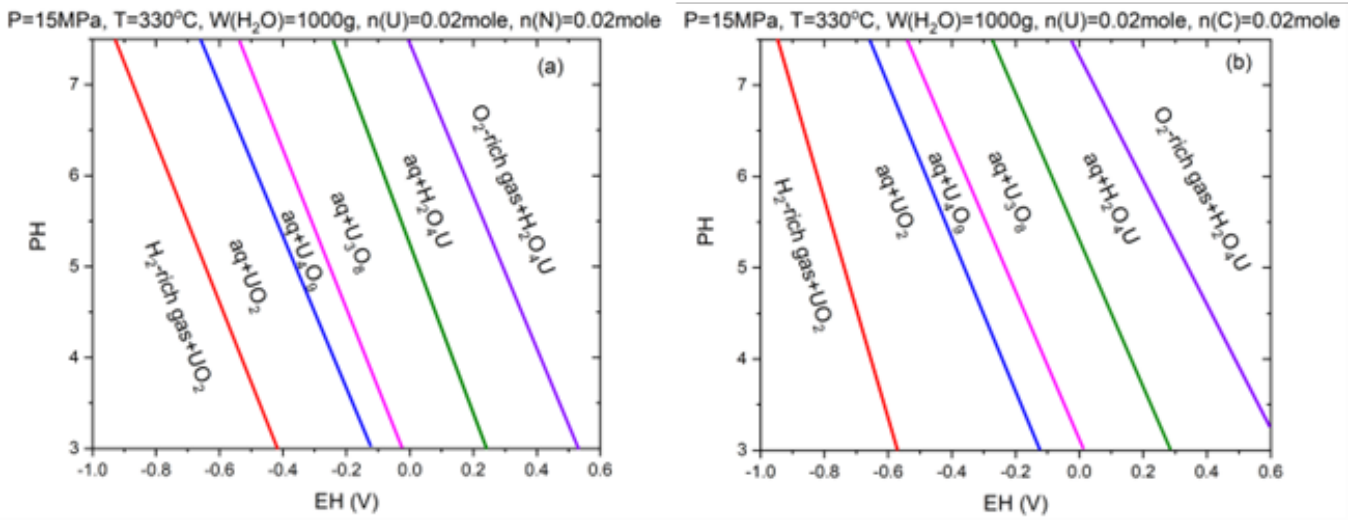

Fig. 2. Calculated pourbaix diagram under the pressurized water reactor (PWR) environment for (a) UN and (b) UC.

the C_2 species. The βUC_2 phase was described by the same model as the (U,Zr)C phase, as they have the same crystal structure. We name them differently to denote their different compositions. The isothermal section at 1700 °C (solid line) calculated from optimized parameters is compared with the experimental postulation [41] (dash line) in Fig. 3(a). The different line colors in the calculated phase diagram denote different phase equilibria: red for three-phase, green for two-phase (tie line) and black for single-phase region. The calculated 1700 °C isothermal section shows that ZrC and UC form a continuous solid solution, and the ZrC content in the (U,Zr)C solid solution that is in equilibrium with graphite and βUC_2 is around 61 ± 3 mol %, which is in a good agreement with the experimental data at 1700 °C. On the other hand, the calculated ZrC liquidus in the isopleth section of the βUC_2–ZrC has higher temperatures than the experimentally postulated one as shown in Fig. 3(b). The calculated liquidus is more reliable as it converges better with the melting temperature of ZrC (around 3500 °C). Adjusting ternary interaction parameters to force exact agreement with the ZrC liquidus lines would compromise binary consistency and distort melting temperature of ZrC anchored in the Zr–C binary system. The calculation also shows the ZrC content in (U,Zr)C solid solution at temperatures higher than 1700 °C are smaller than those estimated from experiment, as shown from the comparison between the calculated and experimental isopleth section of the βUC_2–ZrC in Fig. 3(b). Attempting to better fitting the experimental ZrC in equilibrium with Gra and βUC_2 makes the temperature of invariant reaction Liq → (U,Zr)C + Gra + βUC_2 much higher than the experimental proposed value (2410 °C). In addition, the calculated Liq + (U,Zr)C + Gra three-phase region is smaller than the experimental postulation. It should be noted the experimentally postulated pseudo-binary phase diagram is not a true representation of the βUC_2–ZrC isopleth section. This is because neither UC nor ZrC are strict stoichiometric compounds, and the UC–ZrC pseudo binary can not be uniquely defined and can have slightly different phase boundaries depending on where the isopleth is cut. In this work, we chose $U_{0.5}C_{0.5}$ and $Zr_{0.54}C_{0.46}$ as the two end compositions which were defined by the congruent melting points in respective binaries. The calculated UC–ZrC pseudo binary is compared with experimental data in Fig. 3(c). The calculated results are in reasonable agreement with experimental data given the large uncertainties for high temperature measurements.

2. *The U–Si–C ternary*

The U–Si–C system has been reviewed by Rogl and Noël [45]. They found two ternary compounds in the U–Si–C system: $U_3Si_2C_2$ and $U_{20}Si_{16}C_3$, based on Alekseeva's work [46]. Their Gibbs energy functions cannot be obtained from extrapolation as they do not exist in the constituent binaries. Both phases were found have negligible non-homogeneity range, and therefore were modeled as line compounds. Both phases were found to be thermodynamically stable in 950, 880, and 800 °C isothermal sections. They were reported to form via peritectic reactions from the liquid at about 1750 °C ($U_3Si_2C_2$) and 1600 °C ($U_{20}Si_{16}C_3$), respectively, based on the differential thermal analysis measurements [47]. The Gibbs energy of formation for $U_3Si_2C_2$ was estimated as $\Delta G_f^0 = -355{,}000 \pm 50{,}000(\mathrm{J/mol})$ by Holleck [48] and Pöttgen [49]. Using the above experimental information as constraints, the model parameters in the Gibbs formation energy of $U_3Si_2C_2$ and $U_{20}Si_{16}C_3$ were optimized as $\Delta G_f^0 = -327{,}783 - 26.76 \times T(\mathrm{J/mol})$ for $U_3Si_2C_2$ and $\Delta G_f^0 = -1{,}706{,}860 - 180 \times T(\mathrm{J/mol})$. For other phases emanated from constituent binary systems, their Gibbs energy functions were obtained through extrapolation. The isothermal sections at 950 and 800 °C calculated from the current thermodynamic functions are shown in Fig.4 and in good agreement with the assessed phase diagrams in literature [45]. The calculation suggested $U_3Si_2C_2$ is formed through

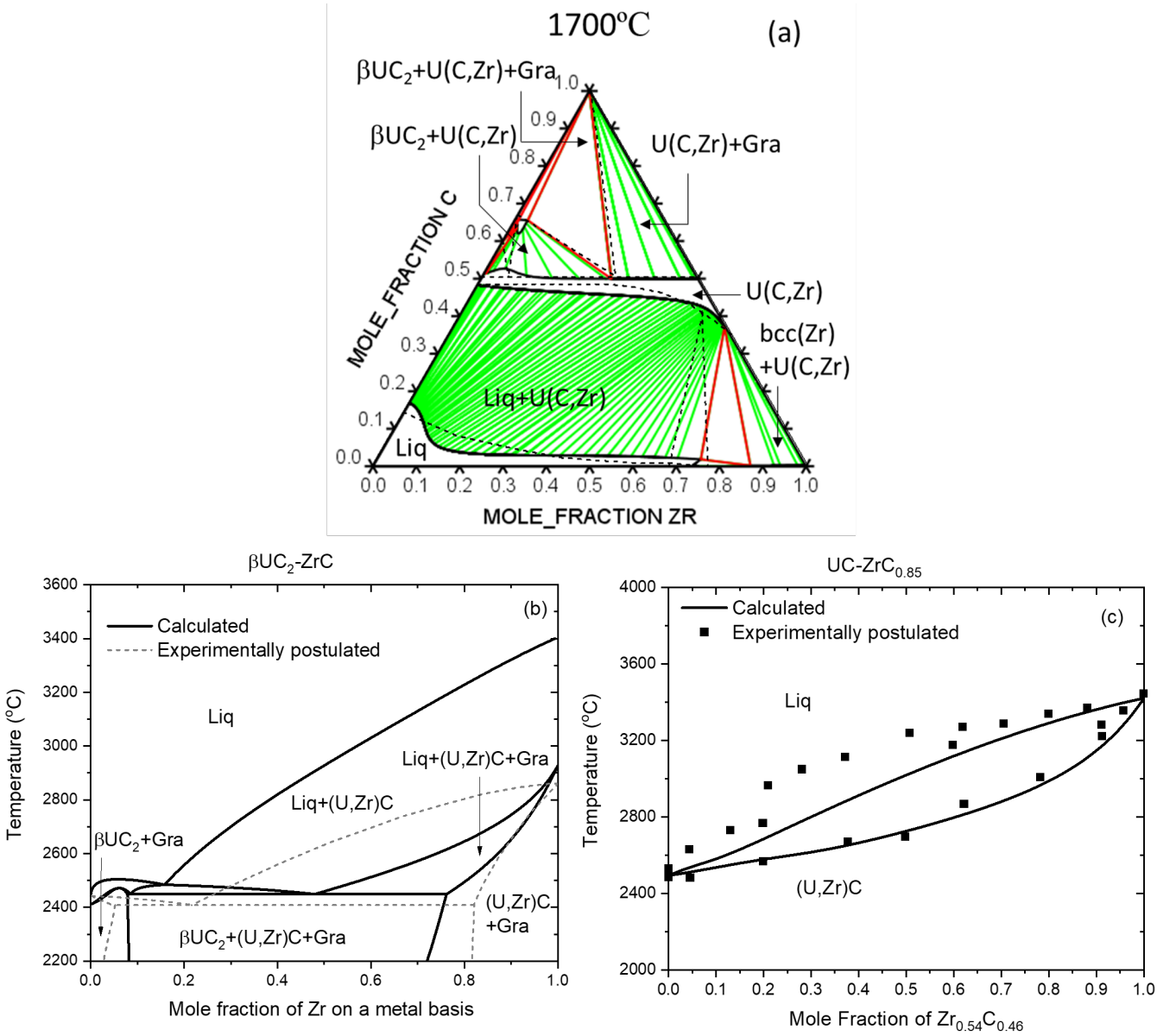

Fig. 3. Comparison between the calculated (a) isothermal section at 1700 °C and that proposed by Perrot [41], (b)isopleth of βUC_2–ZrC and that proposed by Butt [40] and (c) pseudo binary of UC–$ZrC_{0.85}$ and that proposed by Butt [40].

the peritectic reaction of Liquid + UC → $U_3Si_2C_2$ at 1777 °C and the formation of $U_{20}Si_{16}C_3$ is through another peritectic reaction of Liquid + UC → $U_{20}Si_{16}C_3$ at 1619 °C. Isothermal sections calculated at both temperatures are in reasonable agreement with the experimental measurements [45]. In this work, phase equilibrium data at 1750, 1600, 950, 880, and 800 °C were used to constrain only two fitting parameters (ΔH and ΔS), thereby improving confidence in the optimized thermodynamic description while minimizing the number of adjustable variables.

The uncertainty and confidence level of the optimized ternary interaction parameters in U–Zr–C and U–Si–C systems were assessed based on their ability to consistently reproduce experimentally observed phase equilibria across a broad temperature range. While exact statistical confidence intervals are not available due to the intrinsic uncertainty of high-temperature ternary data, the ability to maintain consistent agreement across a wide temperature window provides a practical measure of parameter robustness.

C. Prediction of isothermal section at 1500, 1000, and 500 °C

The calculated Isothermal sections of U–Zr–C at 1500, 1000, and 500 °C are shown in Fig. 5(a–c), together with those of U–Zr–N at 1500, 1000, and 500 °C in Fig. 5(d–f), respectively.

The calculated Isothermal sections of U–Si–C at 1500,

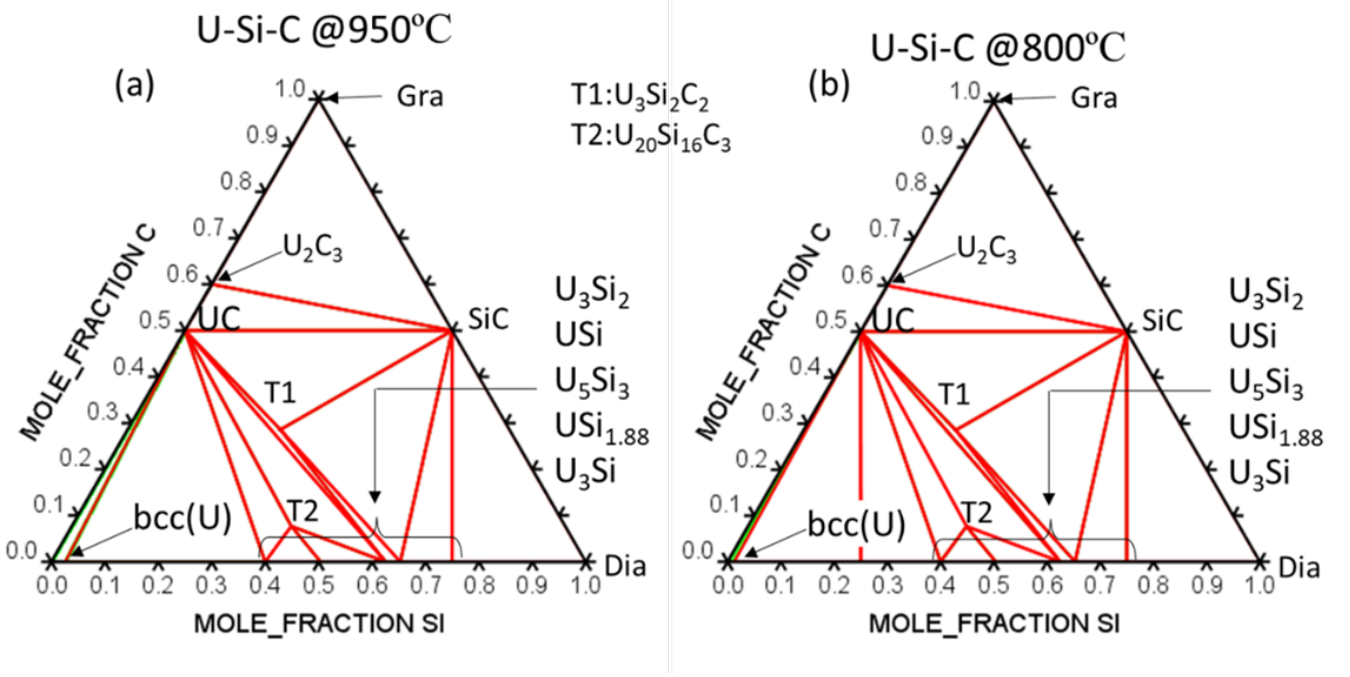

Fig. 4. Calculated Isothermal section at 950 and 800 °C in good agreement with experimental data [45] (not shown here).

1000, and 500 °C and U–N–SiC at 1500, 1000, and 500 °C are shown in Fig. 6 in sequence. The triangles in isothermal sections of a ternary system denote tie-triangle where vertices represent the compositions of phase that are in equilibrium. They are denoted in red in Fig. 6(a–c). On the other hand, the triangle in the quarternary of U–N–Si–C is a section of tie-tetrahedron at isothermal conditions, and they are not necessarily tie triangles.

Quantitatively, the agreement between calculation and experiment for the validated subsystems supports confidence in the extrapolated descriptions: the calculated ZrC content in the (U,Zr)C solid solution in equilibrium with graphite and βUC_2 at 1700 °C is 61 ± 3 mol%, in good agreement with the experimentally assessed value, and the optimized U–Si–C ternary description reproduces the peritectic formation temperatures of $U_3Si_2C_2$ and $U_{20}Si_{16}C_3$ to within the reported experimental uncertainty using only two adjustable parameters. Because the U–N–Zr and U–N–Si–C systems are constructed from constituent binaries—including the nitrogen-containing binaries U–N, Zr–N, and Si–N—that are independently validated against experimental phase boundaries, the predictions for these higher-order systems inherit this quantitative consistency, and any residual uncertainty is therefore bounded by the constituent subsystems rather than introduced by unconstrained ternary parameters. Furthermore, although no isothermal ternary phase-equilibrium data are available for direct optimization of the U–N–Zr system, the predicted U–N–Zr interfacial phase sequence is independently corroborated by historic diffusion-couple measurements of UN against Zircaloy [50], in which the phase assemblages bcc(U,Zr) + hcp(Zr,N) + UZr_2 and bcc(U,Zr) + (U,Zr)N were experimentally identified, in agreement with the phases predicted here. This consistency with an independent experimental observation provides direct, if qualitative, support for the predicted U–N–Zr equilibria beyond the constituent-subsystem validation.

IV. DISCUSSION

A. Response of UN or UCN to cladding breach

Most monolithic uranium-bearing fuel materials of relevance to power reactor applications will pulverize to uranium oxide powder under oxidizing conditions [51]. The calculated Pourbaix diagram indicates that neither UN nor UC is thermodynamically stable in any aqueous electrochemical system during a cladding breach, which cannot be overcome by modifications to coolant chemistry. The stabilities of both UC and UN are similar, suggesting that residual carbon content in UCN would not be expected to impact the response.

Minimal data exists in the open literature describing the reaction of UC or UN with supercritical water, but the limited data reports pulverization of UN to oxides following short time periods [12]. A more extensive database exists regarding the reaction of UN with partial pressures of steam below 1 atm, all universally reporting rapid pulverization above approximately 300 °C [52].

The regions of phase stability shown in Fig. 2 correspond to thermodynamic equilibrium and cannot be used to infer

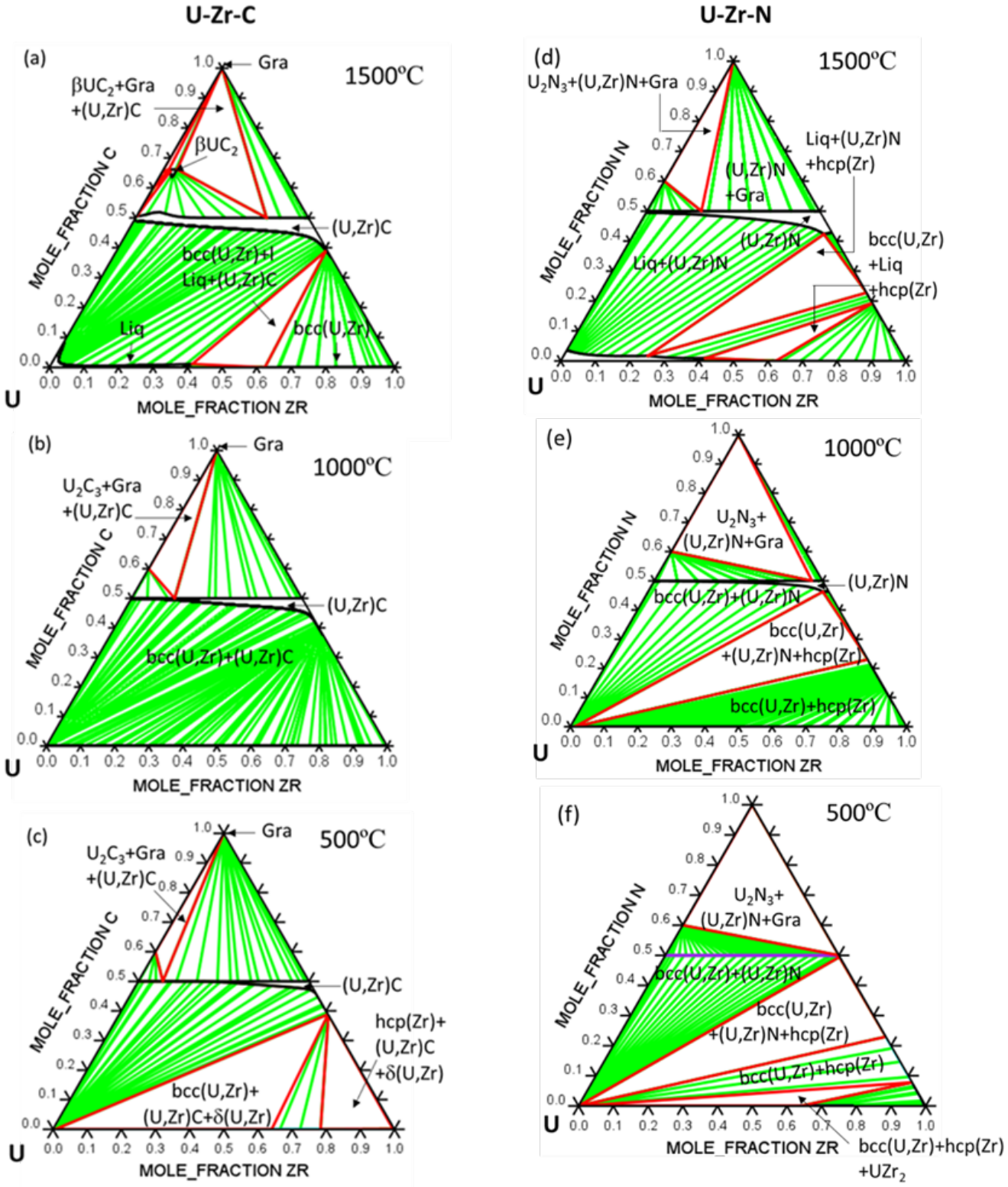

Fig. 5. Predicted isothermal sections of (a, b, c) U–Zr–C at 1500, 1000, and 500 °C, (d, e, f) U–Zr–N at 1500, 1000, and 500 °C, respectively.

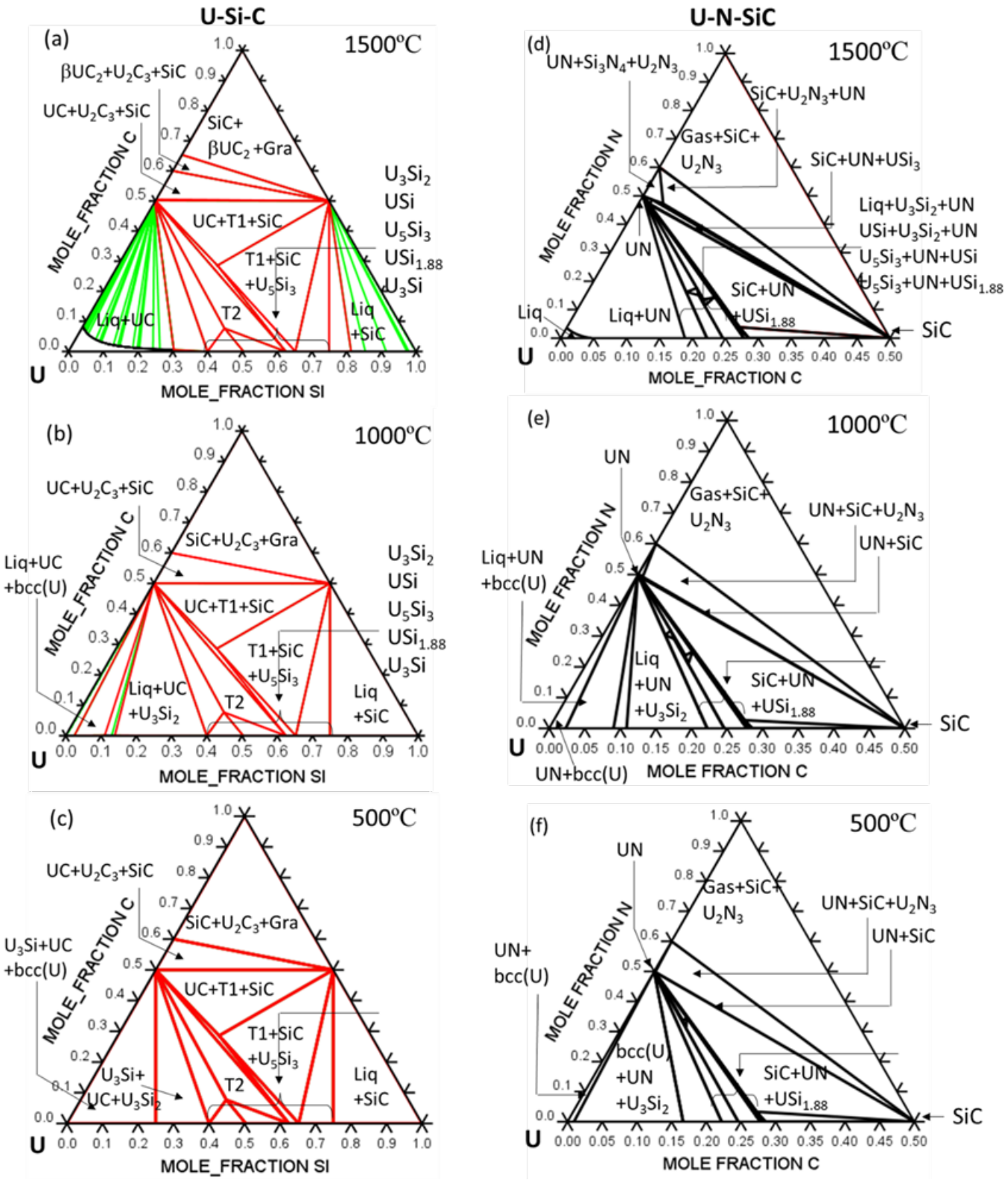

Fig. 6. Predicted isothermal sections (a, b, c) U–Si–C at 1500, 1000, and 500 °C, and (d, e, f) U–N–SiC at 1500, 1000, and 500 °C, respectively.

kinetics of the constituent reactions or potential intermediate phases (e.g., formation of intermediate oxides prior to U_3O_8). An additional consideration when interpreting the results of fundamental thermochemical models is the presence of other phase morphologies that may impact kinetics. For example, thin oxide layers will undoubtedly be present on the surface of any UCN fuel form that is exposed to air during handling or storage [53]. The extent of this layer—potentially as thin as tens of nanometers to as thick as tens of micrometers—may delay exposure of the UN fuel to oxidizing specie resulting from coolant ingress. The most impactful outcome of oxidation of UN pellets during service would be the resulting volume increase. Conversion of UN to UO_2 would progress with swelling of approximately 30%, likely rupturing cladding [2]. Deployment of UN fuels for LWR service therefore requires further study from the experimental community to understand the response of UCN to this anticipated operating occurrence.

B. UN and UCN contact with Zr and SiC during normal operation

Commercial LWR fuel consists of UO_2 clad with a zirconium alloy. Fabrication requires a slight gap to facilitate pellet loading, but more importantly fuel swelling during reactor service must also be accommodated [54]. Fuel–cladding contact in newly inserted fuel typically occurs within the first cycle of reactor operation due to pellet expansion and cladding creep down in PWRs [55]. The cladding then remains in contact with the fuel for the remainder of its service life, generally several years. This extended time spent at 300–350 °C results in the formation of a zirconium dioxide interaction layer 10–30 μm thick [56]. This layer minimally impacts fuel performance during reactor operation but can have impacts on used fuel handling and storage [57].

Given the limited integral irradiation test data available for UN and Zr or SiC cladding, experimental observations are not available. Use of UN in a PWR with Zr alloy cladding is anticipated to experience fuel–cladding contact, but the timing will require integral fuel testing or improved data on swelling of UN pellets irradiated under LWR conditions. Creep down of Zr is likely to be similar for UN fuel as occurs for UO_2 fuel. However, thermal expansion and radial relocation of UN pellets during service should be reduced compared to UO_2 given the lower fuel temperatures provided by increased thermal conductivity [9] and reduced coefficient of thermal expansion [58]. Consideration of a UN–SiC LWR fuel requires more extrapolation. SiC cladding would be expected to see much less deformation during PWR service [59]. Fuel performance modeling performed to assess the response of a UN–SiC fuel during anticipated PWR service confirms projections, as no gap closure is expected [39, 60]. Previous analysis of a U_3Si_2–SiC PWR fuel concept concluded that an expanded fuel–cladding gap would be important to reduce the failure probability of the SiC cladding due to pellet–cladding mechanical interaction under a power ramp [61]. This probable design constraint of UN–SiC LWR fuels coupled with the results of this investigation suggests that deleterious interactions predicted for UN fuel during normal operation should be weighed more heavily if considered for Zr cladding than a future SiC-clad PWR fuel concept.

Based on the calculated isothermal sections of U–Zr–C and U–Zr–N at 500 °C, the interface between UN or UC and Zr is not thermodynamically stable. A UC–Zr interface would promote the formation of the ZrC interlayer, leading to the trilayer structure of Zr/ZrC/UC. This is because the Zr forms the tie-line with ZrC. It is anticipated that a sharp interface will be present between Zr and ZrC. Once the ZrC is formed, gradual transition and interdiffusion between ZrC and UC is expected because the UC and ZrC have the same crystal structure and can form a continuous solid solution. The presence of small quantities of ZrC at the interface of a UCN–Zr fuel form would not be expected to degrade performance, as ZrC is a well understood nuclear material in its own right [62].

Reactions predicted at the interface of UN–Zr are more complicated. First, a significant amount of N can dissolve into Zr to form hcp(Zr,N). This is in contrast to the Zr–C system, where the C solubility in hcp(Zr) is very small. The immediate phase that is in equilibrium with hcp(Zr,N) is UZr_2, suggesting the UZr_2 phase adjacent to the hcp(Zr,N) would be expected, and then the next phase equilibrium adjacent to UZr_2 is hcp(Zr), bcc(U,Zr), or a three-phase mixture of bcc(U,Zr) + UZr_2 + hcp(Zr,N). Finally, a layer with a three-phase mixture of bcc(U,Zr) + hcp(Zr,N) + (U,Zr)N is predicted before transitioning to bulk UN. The calculation results are consistent with historic diffusion couple investigation of UN and Zircaloy, where the interlayers of bcc(U,Zr) + hcp(Zr,N) + UZr_2 and bcc(U,Zr) + (U,Zr)N were observed experimentally [50]. The UZr_2 was the product from the eutectoid reaction bcc(U,Zr) → hcp(Zr,N) + UZr_2, which suggests the kinetics of the UZr_2 formation may be slow.

The major difference predicted between UC–Zr and UN–Zr interfaces at 500 °C is a more complicated reaction pathway in the latter fuel/cladding combination. The C in UC, instead of dissolving into the hcp(Zr), prefers to form ZrC. The ZrC forms a continuous solid solution with UC, leading to a relatively simple reaction pathway. On the other hand, the N in UN will dissolve into the Zr to form hcp(Zr,N), leading to the phase equilibrium of UZr_2 + hcp(Zr,N). The UZr_2 is not in equilibrium with UN, leading to a more complicated reaction pathway across several phase equilibria (e.g., bcc(U,Zr) + UZr_2 + hcp(Zr,N), bcc(U,Zr) + hcp(Zr,N) + (U,Zr)N) As the motivation of the present work is primarily investigation of UCN/Zr where the carbon is present as a processing impurity of the targeted UN fuel form, residual carbon is not predicted to have an impact on fuel–cladding stability. The opposite is predicted, as higher carbon contents in a UCN fuel may be capable of encouraging formation of a more stable ZrC interlayer. A more rigorous assessment of the U–Zr–C–N quaternary is needed to assess this hypothesis, but is beyond the scope of the present work.

For the UN–SiC and UC–SiC fuel–cladding combinations, our calculation results suggested that both UC or UN are in thermodynamic equilibrium with the SiC cladding. Unlike ZrC and ZrN, which form continuous solid solutions with UC and UN, respectively, SiC has a different crystal structure

as UC and UN. Mutual solubility between SiC and UC (or UN) is negligible. Intimate contact between either UC or UN and SiC is not be expected to result in an interfacial reaction and diffusion would not happen at these two temperatures. In addition, as there is no mutual solubility in the UC/SiC and UN/SiC intersection; any deviation of C or N from the stoichiometric ratio (1:1) of UC or UN would lead to the formation of the third phase such as graphite, T1($U_3Si_2C_2$), βUC_2, U_2C_3, and U–Si intermetallic phases. While these phases may be present in a small amount at the fuel–cladding interface if driven by C or N content, it is likely that nonstoichiometry of UCN fuel forms would pose a greater concern to fission product thermochemistry and other more critical aspects of fuel performance [63, 64].

In the present work, UCN is treated as a single U(C,N) solid-solution phase formed by carbon substitution for nitrogen in UN. Thermodynamic calculations confirm that U(C,N) exists as a continuous single-phase solid solution across the composition range between UN and UC at temperatures relevant to this study, consistent with literature assessments [65]. The U(C,N) phase is therefore predicted to remain as a continuous single-phase solid solution over the composition and temperature ranges relevant to this study; fuel–cladding interaction is governed primarily by thermodynamic interactions with cladding materials rather than phase transformation within the fuel.

It should be noted that the predicted thermodynamic compatibility between UC/UN and SiC cladding reflects equilibrium conditions in the absence of irradiation. Under reactor service conditions, irradiation-induced defect generation and radiation-enhanced diffusion in SiC may modify interfacial kinetics and alter the effective transport of species across the fuel–cladding interface [39, 60]. While direct experimental data resolving UC/UN–SiC chemical interactions under neutron irradiation remain limited—most existing studies having focused on the thermomechanical response of SiC cladding [59]—the thermodynamic driving forces identified here provide a necessary baseline for future coupled thermodynamic–kinetic modeling and experimental investigation of irradiation effects on fuel–cladding compatibility.

C. UN and UCN contact with Zr during accident conditions

The rate, extent and duration of temperature increase of LWR fuel and cladding materials following a design-basis loss of coolant or reactivity insertion accident (LOCA and RIA, respectively) depend on the specific conditions of the scenario [66]. During a LOCA, cladding and temperatures can exceed 1000°C without recovery or intervention of an emergency core cooling systems [67, 68]. The U.S. Nuclear Regulatory Commission does not allow LWR peak cladding temperature to exceed 1204 °C, or be subjected to time at temperature such that oxide thickness exceeds 17% of the total cladding thickness prior to oxidation [69]. Contemporary Zr alloys are capable of tolerating steam oxidation at 1000–1100 °C for time periods of 1000–10,000 s before the oxide thickness criterion is exceeded, depending on the alloy composition and other environmental factors [70].

Based on the calculated isothermal sections, if UC or UN are directly in contact with Zr above 1000 °C, the interface would proceed into the phase regions involving bcc(U,Zr) solid or liquid phases. Pure U melts at 1130 °C, and increasing Zr content gradually increases the solidus. The formation of a liquid phase at the fuel–cladding interface would be detrimental to understanding and predicting accident performance. During a LOCA as outlined above, Zr cladding will balloon in multiple locations due to the increasing internal pressure of the fuel rod, resulting in “lift-off” of the cladding and separation of any bond that may have formed between the fuel and cladding [71, 72]. The (U,Zr) phases that formed during steady state operation will remain, and the presence of a complex multiphase structure as discussed in Section IV B may complicate prediction of where cladding lift-off occurs during ballooning, potentially introducing a stochastic process. However, prolonged intimate contact between UN and Zr would not be anticipated under a design-basis LOCA. The presence of carbon as an impurity in UCN is again predicted to be either neutral or potentially beneficial through encouragement of ZrC formation similarly to normal operating conditions when modeled at 1000 °C. However, this effect is no longer present at 1500 °C where a more complex interface including a liquid (U,Zr) constituent is predicted similarly to the U–N–Zr system.

Extrapolation of these results to consideration of LOCA or RIA conditions produces similar conclusions. The relevant timescales to a RIA are seconds at most, but during this brief time fuel temperatures in the UO_2–Zr system can exceed 2000 °C and surpass the 2850 °C melt point of UO_2 [73]. The extreme temperatures induced by a RIA would therefore increase the likelihood that lower melting point phases present at the fuel–cladding interface experience melting, but the limited time spent at these temperatures will limit further interdiffusion between the fuel and cladding if they are in contact.

The response of irradiated SiC cladding containing irradiated fuel to LOCA or RIA conditions is speculative. The reduced ductility of SiC cladding compared to Zr suggests that any contact between SiC and UN may persist to higher temperatures during a transient, as ballooning is not observed during LOCA testing of SiC [74]. This provides a greater potential for interdiffusion between SiC cladding and fuel at elevated temperature, but in the case of UN no new deleterious interactions emerge. The interface between UN and UC and SiC at temperatures above 1000 °C is predicted to be similar to that at normal operation conditions because of similar phase equilibrium as shown in Fig. 6(d–f). The formation of free uranium is not predicted following assessment of SiC cladding interactions with UN regardless of carbon content. Any uranium carbide or uranium silicide phases that may form at elevated temperatures pose less of a concern for short term reactor accident scenarios given their higher melting points.

D. Potential strategies for mitigating UCN–Zr interactions

The present study predicts use of UN with SiC cladding to be far less of a concern compared to use of UN with Zr cladding when judged from the standpoint of potential fuel–cladding interactions. Contact between UN and UCN with Zr in a PWR is anticipated to occur during anticipated service conditions, and is predicted to result in a complex interface structure, as shown in a calculated isopleth between fuel U($C_{0.3}N_{0.7}$) and pure Zr. At lower temperatures, the U($C_{0.3}N_{0.7}$)/Zr interface is predicted to form complex phases such as bcc(U,Zr) metal solution phases in bcc, tetragonal or orthorhombic structures, UZr_2 intermetallic, phase separation of fcc (U,Zr)(C,N) into Zr-rich and U-rich compositions, and high N containing hcp(Zr). If substantiated by experimental findings, these behaviors will be difficult to account for to predict fuel performance during service and eventual transport, storage, and disposition.

Thermal transients as anticipated during design-basis and beyond design-basis accidents are predicted to result in the formation of (U,Zr) compositions that will melt if temperatures exceed 1130 °C. The presence of these phases poses more of a challenge for management of a RIA rather than a LOCA, as Zr oxidation would still likely dominate allowable time spent above 1000 °C. Pairing of UN with a coated Zr cladding concept may create more of a driver to understand the behavior of interfacial phases formed due to fuel–cladding interactions given the ability of chromium coatings to limit oxidation at high temperatures [75]. However, data collected to date indicate coatings do not significantly impact burst behavior, suggesting that cladding lift-off would be comparable to uncoated Zr [76].

The results of the present work enable assessment of potential means to mitigate these deleterious interactions between UN and Zr. Figure 7 plots isopleth sections of U($C_{0.3}N_{0.7}$), chosen as a composition representative of high carbon content present as an impurity in contemporary UN [77]. Figure 7(a) depicts the complex phase transition predicted for UC or UN (specifically U($C_{0.3}N_{0.7}$) here) in contact with Zr, which are consistent with the three isothermal sections in Figure 5. Prediction of multiphase interdiffusion regions persist until temperature exceeds 600 °C, where formation of bcc(U,Zr) dominates, as shown in Fig. 7(a).

However, the isopleths plotted in Fig. 7(b–c) highlight a different response when U($C_{0.3}N_{0.7}$) is evaluated in contact with ZrC and ZrN, respectively. Thermodynamically, an interlayer of ZrC or ZrN between Zr and UN would reduce the reaction at interface to produce (U,Zr). This can be observed in the large mutually miscible region between U($C_{0.3}N_{0.7}$) and ZrC or ZrN. The mutual solubility between U($C_{0.3}N_{0.7}$) and ZrC or ZrN can ensure a good bonding between fuel and cladding without forming detrimental phases at the interface while also avoiding the formation of low melting point metal phase.

ZrC may be a superior choice for a coating to achieve this goal. ZrN is in equilibrium with hcp(Zr,N) as shown in Fig. 5(d); a thin layer of ZrN deposited on Zr could potentially degrade if N dissolves into the Zr bulk. This behavior has been observed experimentally; ten micrometer ZrN layers deposited on Zr were found to dissolve into the bulk when annealed at temperatures above 1200 °C for even brief (minute) time periods [78]. However, annealing performed at 900 °C for extended time intervals found that the ZrN layer remained. Conversely, C solubility in Zr is small, therefore the ZrC deposited on Zr should not cause the degradation of Zr, and can serve as a better interlayer to protect the Zr cladding. Further testing is needed to evaluate the relevant kinetics at temperatures in the 400–500 °C temperature range where a ZrN or ZrC layer would need to persist for years in order to serve an intended function of preventing (U,Zr) and UZr_2 formation at an interface between UCN fuel and Zr cladding.

As interfacial reaction kinetics is more of concern at high temperatures where the reaction kinetics is faster, the allowable temperature range for ZrN should stay below 900 °C and that for ZrC can be higher and up to 1100 °C, based on both thermodynamic modeling and literature results. Compared to the Cr-based coatings that are currently proposed for accident tolerant fuel (ATF) development, ZrC or ZrN coatings can eliminate the thermodynamic driving force for (U,Zr) metallic phase formation if direct fuel–cladding contact occurs, while Cr-based coatings primarily function as oxidation barriers that significantly improve high-temperature steam resistance during LOCA scenarios. Therefore, the Cr coatings can not fundamentally modify fuel–cladding chemical compatibility in the same manner as ZrC or ZrN interlayers.

E. Design implications for LWR fuel development

The thermodynamic results of this study provide several important implications for advanced LWR fuel design. First, direct pairing of UN with Zr-based cladding is predicted to produce a complex, multiphase interdiffusion region which increases uncertainty in long-term interfacial stability and potentially leads to formation of low-melting (U,Zr) phases at elevated temperatures. ZrN coatings, while potentially beneficial at moderate temperatures, may degrade at high temperature due to N solubility in Zr and dissolution of the nitride layer. In contrast, ZrC interlayers are thermodynamically attractive because carbon preferentially forms ZrC rather than dissolving extensively in Zr, enabling formation of a stable barrier that suppresses deleterious (U,Zr) metallic phases. SiC cladding exhibits intrinsic thermodynamic compatibility with both UN and UC, with negligible mutual solubility and no driving force for formation of low-melting metallic phases, thereby offering a fundamentally more stable fuel–cladding pairing. Finally, while C impurities in U(C,N) are not predicted to be detrimental, the carbon content should be specified within defined design envelopes, as stoichiometry influences interfacial phase equilibria and may affect barrier-layer formation behavior.

F. Limitations of the equilibrium thermodynamic approach

The present study is based on equilibrium thermodynam-

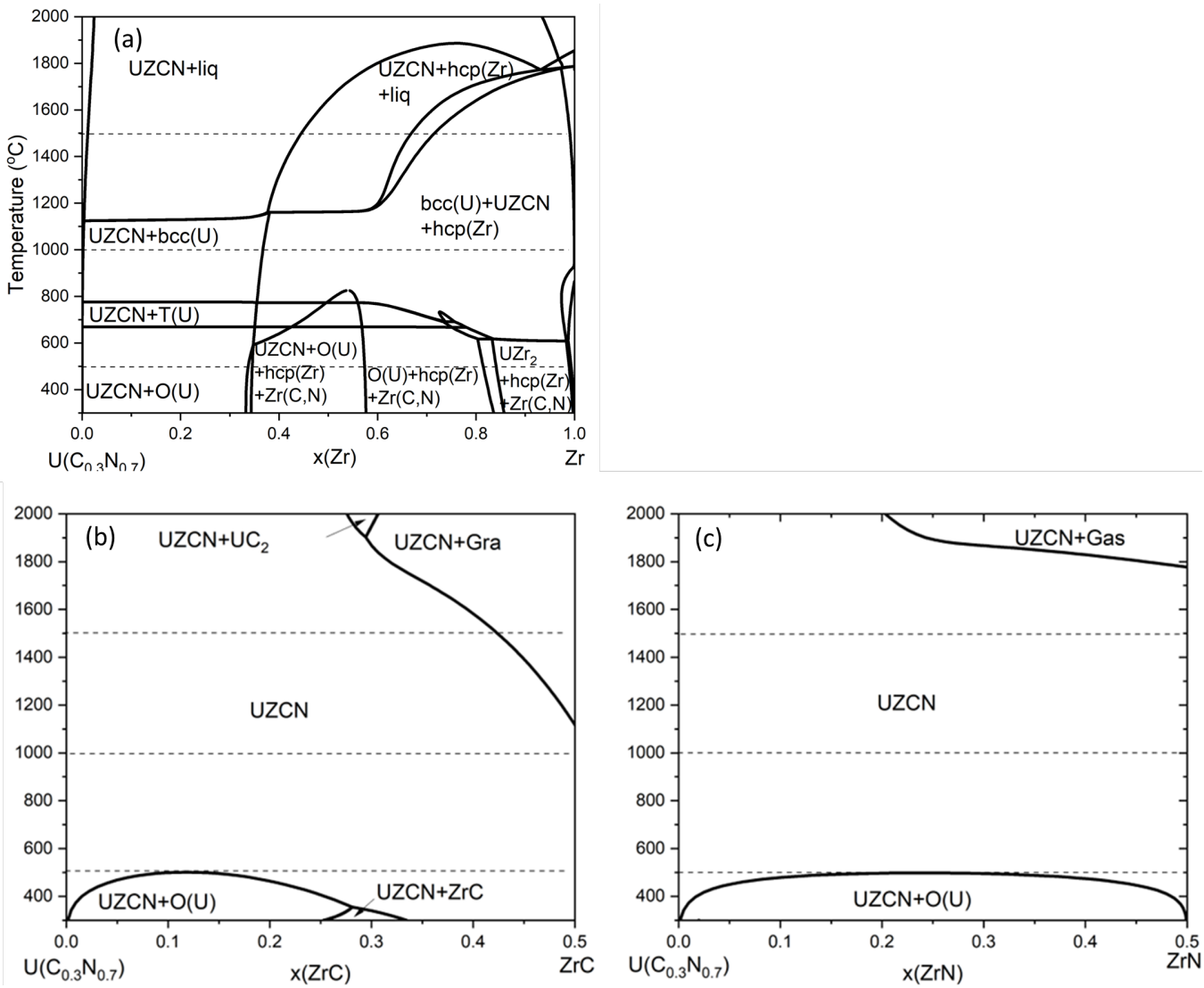

Fig. 7. Calculated isopleth sections of (a) $U(C_{0.3}N_{0.7})$–Zr, (b) $U(C_{0.3}N_{0.7})$–ZrC, and (c) $U(C_{0.3}N_{0.7})$–ZrN. UZCN denotes the abbreviation of fcc (U,Zr)(C,N) phase. The three dash lines denote the temperature at 500, 1000, and 1500 °C, respectively.

ics and therefore does not explicitly account for kinetic effects that govern the actual rate and extent of fuel–cladding interactions under reactor service conditions. Fuel–cladding interaction is kinetically controlled, and the equilibrium phase assemblages predicted here represent the thermodynamically favored end states rather than the transient or metastable phases that may form and persist under operating conditions.

Specifically, the following kinetic phenomena are not captured by the present analysis: (1) interdiffusion kinetics at the fuel–cladding interface, which control the rate of phase layer growth; (2) irradiation-enhanced diffusion, which can significantly accelerate species transport and phase boundary migration compared to thermally driven diffusion alone; (3) the nucleation and growth kinetics of reaction product phases, including the possible stabilization of metastable phases; and (4) the influence of fission products, point defect populations, and microstructural evolution on interfacial chemistry.

Despite these limitations, equilibrium thermodynamic analysis provides a necessary foundation by identifying the thermodynamically accessible phase space, defining the chemical driving forces for interfacial reactions, and establishing which phases are stable or metastable under given conditions. The equilibrium results serve as a baseline for non-irradiated conditions and provide essential input for future coupled thermodynamic–kinetic models (e.g., DICTRA-type diffusion simulations) that can incorporate the kinetic phenomena listed above. The predicted phase equilibria should therefore be interpreted as identifying potential reaction products and thermodynamic drivers for interaction, rather than as quantitative predictions of reaction layer thickness or kinetics under specific service conditions.

V. CONCLUSIONS

This study first performed thermodynamic calculation of pure UC and UN in a closed system mimicking PWR coolant. The calculated Pourbaix diagrams of UN and UC under PWR conditions suggest that UN or UC is not thermodynamically stable in any aqueous electrochemical system during a cladding breach, which cannot be overcome by modifications to coolant chemistry. A systematic thermodynamic evaluation was then performed to assess the potential interactions between UN and UCN with Zr or SiC cladding. A thermodynamic database of U–Zr–Si–C–N was developed using the CALPHAD approach and validated with available literature data. The interfacial stability of UN/Zr, UC/Zr, UN/SiC and UC/SiC were assessed by calculating the isothermal sections U–Zr–N, U–Zr–C, U–Si–C, U–Si–C–N at 1500,1000, and 500 °C. The results predict that the interface between the Zr cladding and UCN fuel is not stable at operating temperature (500 °C) and the elevated temperatures chosen to represent transient conditions. The reaction pathway between UN and Zr will produce multiple layers including phases of bcc(U,Zr), UZr_2, hcp(Zr,N) and fcc(U,Zr)N. This response is more complicated than that between UC and Zr where a single ZrC layer is predicted. Formation of (U,Zr) and transient conditions above 1130 °C would have the potential to produce a liquid phase, relevant to understanding of accident behavior of UN-Zr fuel systems. Improved thermodynamic stability is predicted when compatibility with SiC cladding is considered. Both UN and UC are in equilibrium with SiC when modeled under the same temperature conditions. Potential carbon impurities present in UN as a result of the fabrication process were not found to contribute detrimentally to fuel–cladding contact for either Zr or SiC cladding under conditions evaluated here.

VI. ACKNOWLEDGEMENT

The research was partially sponsored by the National Nuclear Security Administration Office of Defense Nuclear Nonproliferation Research and Development (DNN R&D), U.S., Department of Energy (DOE). This research was also partially sponsored by the DOE Office of Nuclear Energy's Advanced Fuels Campaign. This paper is authored by UT-Battelle under Contract No. DE-AC05-00OR22725 with the U.S. DOE. The authors would like to acknowledge Dingwon Shin and Nathan Capps for their technical reviews and comments on this manuscript.

[1] K. Pasamehmetoglu, S. Massara, D. Costa, et al. *State-of-the-Art Report on Light Water Reactor Accident-Tolerant Fuels*. Tech. Rep (Organisation for Economic Co-Operation and Development, France, 2018).

[2] R. T. Sweet, Y. Yang, K. A. Terrani, et al. Performance of U3Si2 in an LWR following a cladding breach during normal operation. J. Nucl. Mater. **539**, 152263 (2020).

[3] J. R. Burns, R. Hernandez, K. A. Terrani, et al. Reactor and fuel cycle performance of light water reactor fuel with 235U enrichments above 5%. Ann. Nucl. Energy **142**, 107423 (2020).

[4] L. Carlson, J. Miller, and Z. Wu. Implications of HALEU fuel on the design of SMRs and micro-reactors. Nucl. Eng. Des. **389**, 111648 (2022).

[5] A. T. Nelson and P. Demkowicz. Other power reactor fuels. In *Advances in Nuclear Fuel Chemistry* (Elsevier, 2020) pp. 215–247.

[6] F. Cappia and J. M. Harp. Postirradiation examinations of low burnup U3Si2 fuel for light water reactor applications. J. Nucl. Mater. **518**, 62 (2019).

[7] J. K. Watkins, A. R. Wagner, A. Gonzales, et al. Challenges and opportunities to alloyed and composite fuel architectures to mitigate high uranium density fuel oxidation: Uranium diboride and uranium carbide. J. Nucl. Mater. **560**, 153502 (2022).

[8] R. Konings and R. E. Stoller, eds. *Comprehensive Nuclear Materials* (Elsevier, 2020).

[9] S. Hayes, J. Thomas, and K. Peddicord. Material property correlations for uranium mononitride: III. transport properties. J. Nucl. Mater. **171**, 289 (1990).

[10] G. Vasudevamurthy and A. T. Nelson. Uranium carbide properties for advanced fuel modeling—a review. J. Nucl. Mater. **558**, 153145 (2022).

[11] K. A. Terrani, N. A. Capps, M. J. Kerr, et al. Accelerating nuclear fuel development and qualification: Modeling and simulation integrated with separate-effects testing. J. Nucl. Mater. **539**, 152267 (2020).

[12] A. T. Nelson, A. Migdisov, E. S. Wood, et al. U3Si2 behavior in H2O environments: Part II, pressurized water with controlled redox chemistry. J. Nucl. Mater. **500**, 81 (2018).

[13] V. Jayaraj, S. Thirunavukkarasu, V. Anandaraj, et al. Evaluation of fuel-clad chemical interaction in PFBR MOX test fuel pins. J. Nucl. Mater. **509**, 94 (2018).

[14] D. D. Keiser. Fuel cladding chemical interaction in metallic sodium fast reactor fuels: A historical perspective. J. Nucl. Mater. **514**, 393 (2019).

[15] K. Nogita and K. Une. Formation of pellet-cladding bonding layer in high burnup BWR fuels. J. Nucl. Sci. Technol. **34**, 679 (1997).

[16] C. Ciszak, L. Desgranges, P. Garcia, et al. On the origins and the evolution of the fuel-cladding bonding phenomenon in PWR fuel rods. J. Nucl. Mater. **520**, 110 (2019).

[17] L. Hallstadius, S. Johnson, and E. Lahoda. Cladding for high performance fuel. Prog. Nucl. Energy **57**, 71 (2012).

[18] C. d. F. Azevedo. Selection of fuel cladding material for nuclear fission reactors. Eng. Failure Anal. **18**, 1943 (2011).

[19] R. E. Hoggan, L. He, and J. M. Harp. Interdiffusion behavior of U3Si2 with FeCrAl via diffusion couple studies. J. Nucl. Mater. **502**, 356 (2018).

[20] R. E. Hoggan, L. He, and J. M. Harp. Erratum to interdiffusion behavior of U3Si2 with FeCrAl via diffusion couple studies. J. Nucl. Mater. **507**, 403 (2018).

[21] H. J. Qu, M. Higgins, H. Abouelella, et al. FeCrAl fuel/clad chemical interaction in light water reactor environments. J. Nucl. Mater. **587**, 154717 (2023).

[22] M. Ben-Belgacem, V. Richet, K. A. Terrani, et al. Thermo-mechanical analysis of LWR SiC/SiC composite cladding. J. Nucl. Mater. **447**, 125 (2014).

[23] C. Deck, G. Jacobsen, J. Sheeder, et al. Characterization of SiC–SiC composites for accident tolerant fuel cladding. J. Nucl. Mater. **466**, 667 (2015).

[24] N. Saunders and A. P. Miodownik. *CALPHAD (Calculation of Phase Diagrams): A Comprehensive Guide* (Elsevier, 1998).

[25] W. E. Acree. Mathematical representation of thermodynamic properties: Part 2. Derivation of the combined nearly ideal binary solvent (NIBS)/Redlich-Kister mathematical representation from a two-body and three-body interactional mixing model. Thermochim. Acta **198**, 71 (1992).

[26] Y. M. Muggianu, M. Gambino, and J. Bros. Enthalpies of formation of liquid alloys bismuth-gallium-tin at 723k—choice of an analytical representation of integral and partial thermodynamic functions of mixing for this ternary-system. J. Chim. Phys. Phys.-Chim. Biol. **72**, 83 (1975).

[27] A. Berche, C. Rado, O. Rapaud, et al. Thermodynamic study of the U-Si system. J. Nucl. Mater. **389**, 101 (2009).

[28] J. Grobner, H. L. Lukas, and F. Aldinger. Thermodynamic calculation of the ternary system Al-Si-C. Calphad **20**, 247 (1996).

[29] C. Guéneau, N. Dupin, B. Sundman, et al. Thermodynamic modelling of advanced oxide and carbide nuclear fuels: Description of the U-Pu-O-C systems. J. Nucl. Mater. **419**, 145 (2011).

[30] A. F. Guillermet. Analysis of thermochemical properties and phase-stability in the zirconium carbon system. J. Alloys Compd. **217**, 69 (1995).

[31] M. Kurata. Thermodynamic assessment of the Pu-U, Pu-Zr, and Pu-U-Zr systems. Calphad **23**, 305 (1999).

[32] X. Y. Ma, C. R. Li, K. W. Bai, et al. Thermodynamic assessment of the Zr-N system. J. Alloys Compd. **373**, 194 (2004).

[33] X. Y. Ma, C. R. Li, F. M. Wang, et al. Thermodynamic assessment of the Si-N system. Calphad **27**, 383 (2003).

[34] H. Okamoto. N-U (nitrogen-uranium). J. Phase Equilib. **18**, 107 (1997).

[35] T. M. Besmann, D. Shin, and T. B. Lindemer. Uranium nitride as LWR TRISO fuel: Thermodynamic modeling of U–C–N. J. Nucl. Mater. **427**, 162 (2012).

[36] H. L. Lukas, S. G. Fries, and B. Sundman. *Computational Thermodynamics: The CALPHAD Method* (Cambridge University Press, Cambridge, UK, 2007).

[37] J.-O. Andersson, T. Helander, L. Höglund, et al. Thermo-Calc & DICTRA, computational tools for materials science. Calphad **26**, 273 (2002).

[38] J. C. Tanger and H. C. Helgeson. Calculation of the thermodynamic and transport properties of aqueous species at high pressures and temperatures; revised equations of state for the standard partial molal properties of ions and electrolytes. Am. J. Sci. **288**, 19 (1988).

[39] W. Li and K. Shirvan. Implications of SiC irradiation creep and annealing to UN-SiC fuel rod behavior. J. Nucl. Mater. **542**, 152479 (2020).

[40] D. P. Butt and T. C. Wallace. The U–Zr–C ternary phase diagram above 2473 K. J. Am. Ceram. Soc. **76**, 1409 (1993).

[41] P. Perrot. C-U-Zr ternary phase diagram evaluation. In *MSI Eureka in SpringerMaterials*. Edited by G. Effenberg (Springer,

2006).
[42] F. Benesovsky and E. Rudy. On the systems U-Zr (Hf, Nb, Ta)-C. Planseeber. Pulvermet **9**, 65 (1961).
[43] H. Holleck. *Ternary phase equilibria in the systems actinide–transition metal–carbon and actinide–transition metal–nitrogen*. Tech. Rep (Kernforschungszentrum, Karlsruhe, Germany, 1975).
[44] H. Nickel, O. Inanc, and K. Lücke. On the knowledge of the U-Zr-C system. J. Nucl. Mater. **28**, 79 (1968).
[45] P. Rogl and H. Noël. The C-Si-U system (carbon-silicon-uranium). J. Phase Equilib. **16**, 66 (1995).
[46] Z. Alekseeva. Phase equilibria in the U-Si-C system. J. Nucl. Mater. **186**, 294 (1992).
[47] P. Guinet, H. Vaugoyeau, J. Laugier, et al. Etude d'un equilibre a 4 phases solides dans le systeme ternaire U–C–Si. J. Nucl. Mater. **21**, 21 (1967).
[48] H. Holleck and H. Kleykamp. Thermodynamics of multicomponent systems containing UC and PuC: A review. J. Nucl. Mater. **32**, 1 (1969).
[49] R. Pöttgen, D. Kaczorowski, and W. Jeitschko. Crystal structure, magnetic susceptibility and electrical conductivity of the uranium silicide carbides U3Si2C2 and U20Si16C3. J. Mater. Chem. **3**, 253 (1993).
[50] D. E. Price, D. Moak, W. Chubb, et al. *The Compatibility of Uranium Nitride with Potential Cladding Metals*. Tech. Rep (Battelle Memorial Institute, Columbus, Ohio, United States, 1966).
[51] R. T. Sweet, K. A. Terrani, B. D. Wirth, and A. T. Nelson. Performance of U3Si2 in LWR following a cladding breach during normal operation. J. Nucl. Mater. **539**, 152263 (2020).
[52] E. S. Sooby, B. A. Brigham, G. Robles, et al. Steam oxidation of uranium mononitride in pure and reducing steam atmospheres to 1200 °C. J. Nucl. Mater. **560**, 153487 (2022).
[53] P. D. Edmondson, Q. B. Smith, J. W. Werden, et al. Scanning transmission electron microscopy characterization of the native surfaces oxides in high density ceramic fuels. Microsc. Microanal. **25**, 1594 (2019).
[54] G. Pastore, L. Luzzi, V. Di Marcello, et al. Physics-based modelling of fission gas swelling and release in UO2 applied to integral fuel rod analysis. Nuclear Engineering and Design **256**, 75 (2013).
[55] N. Capps, M. Kennard, W. Liu, et al. PCI analysis of a commercial PWR using BISON fuel performance code. Nucl. Eng. Des. **324**, 131 (2017).
[56] K.-T. Kim. UO2/Zry-4 chemical interaction layers for intact and leak PWR fuel rods. J. Nucl. Mater. **404**, 128 (2010).
[57] P. Konarski, C. Cozzo, G. Khvostov, et al. Spent nuclear fuel in dry storage conditions—current trends in fuel performance modeling. J. Nucl. Mater. **555**, 153138 (2021).
[58] S. Hayes, J. Thomas, and K. Peddicord. Material property correlations for uranium mononitride: I. physical properties. J. Nucl. Mater. **171**, 262 (1990).
[59] G. Singh, K. Terrani, and Y. Katoh. Thermo-mechanical assessment of full SiC/SiC composite cladding for LWR applications with sensitivity analysis. J. Nucl. Mater. **499**, 126 (2018).
[60] H. Han, J. Liao, R. Liu, et al. Transient fuel behavior analysis of UN fuel with a two-layered SiC cladding based on multiphysics method. Nucl. Eng. Des. **415**, 112723 (2023).
[61] Y. He, K. Shirvan, Y. Wu, et al. Fuel performance optimization of U3Si2-SiC design during normal, power ramp and RIA conditions. Nucl. Eng. Des. **353**, 110276 (2019).
[62] Y. Katoh, G. Vasudevamurthy, T. Nozawa, et al. Properties of zirconium carbide for nuclear fuel applications. J. Nucl. Mater. **441**, 718 (2013).
[63] Y. Arai, T. Iwai, and T. Ohmichi. Chemical state of fission products in irradiated uranium carbide fuel. J. Nucl. Mater. **151**, 63 (1987).
[64] C. Degueldre, D. Goddard, G. Berhane, et al. Simulation of uranium mononitride spent fuel: A thermodynamic approach. J. Nucl. Mater. **592**, 154900 (2024).
[65] P. Perrot. Carbon – nitrogen – uranium: Datasheet from landolt-börnstein - group IV physical chemistry · volume 11e2: "refractory metal systems" in springermaterials. Copyright 2010 Springer-Verlag Berlin Heidelberg. Part of SpringerMaterials. accessed 2026-04-24.
[66] S. J. Zinkle, K. A. Terrani, J. C. Gehin, et al. Accident tolerant fuels for LWRs: A perspective. J. Nucl. Mater. **448**, 374 (2014).
[67] F. Erbacher, S. Leistikow, R. Adamson, et al. Zircaloy fuel cladding behavior in a loss-of-coolant accident: A review. In *Zirconium in the Nuclear Industry* (ASTM International, 1987).
[68] N. Capps, A. Wysocki, A. Godfrey, et al. Full core LOCA safety analysis for a PWR containing high burnup fuel. Nucl. Eng. Des. **379**, 111194 (2021).
[69] Acceptance criteria for emergency core cooling systems for light-water nuclear power reactors. Code of Federal Regulations 10 CFR 50.46 (2021).
[70] J. H. Baek and Y. H. Jeong. Breakaway phenomenon of Zr-based alloys during a high-temperature oxidation. J. Nucl. Mater. **372**, 152 (2008).
[71] V. Brankov, G. Khvostov, K. Mikityuk, et al. Analysis of effects of pellet-cladding bonding on trapping of the released fission gases in high burnup KKL BWR fuels. Nucl. Eng. Des. **305**, 559 (2016).
[72] L. Ammirabile and S. Walker. Multi-pin modelling of PWR fuel pin ballooning during post-LOCA reflood. Nucl. Eng. Des. **238**, 1448 (2008).
[73] L. O. Jernkvist. Computational assessment of burnup-dependent fuel failure thresholds for reactivity initiated accidents. J. Nucl. Sci. Technol. **43**, 546 (2006).
[74] K. Kane, S. Bell, N. Capps, et al. The response of accident tolerant fuel cladding to LOCA burst testing: A comparative study of leading concepts. J. Nucl. Mater. **574**, 154152 (2023).
[75] M. Steinbrück, U. Stegmaier, M. Große, et al. High-temperature oxidation and quenching of chromium-coated zirconium alloy ATF cladding tubes with and w/o pre-damage. J. Nucl. Mater. **559**, 153470 (2022).
[76] S. B. Bell, T. Graening, A. Evans, et al. Burst and oxidation behavior of Cr-coated Zirlo during simulated LOCA testing. J. Nucl. Mater. **564**, 153679 (2022).
[77] T. B. Lindemer, C. M. Silva, J. J. Henry, et al. Quantification of process variables for carbothermic synthesis of UC1-xNx fuel microspheres. J. Nucl. Mater. **483**, 176 (2017).
[78] J. Yang, Y. Ding, F. Zhao, et al. Diffusion and oxidation behavior of Cr-ZrN coated Zr alloy accident tolerant fuel cladding materials at high temperature. Surf. Coat. Technol. **476**, 130246 (2024).